Supporting Material for "A stochastic model of calcium puffs based on single channel data"

Pengxing Cao[1], Graham Donovan[1], Martin Falcke[2], and James Sneyd*[1]

[1]Department of Mathematics, The University of Auckland, Auckland, New Zealand
[2]Mathematical Cell Physiology, Max Delbrück Center for Molecular Medicine, Berlin, Germany

*Correspondence: sneyd@math.auckland.ac.nz

Contents

The supporting material contains the following:

Summary of equations and parameters of the IP_3R model

In the main text, we have introduced the Siekmann IP_3R model which is a 6-state Markov model derived from stationary single channel data (see Fig. 1). All the rates of state-transition are constants (given in Table S1) except q_{24} and q_{42} which are Ca^{2+}-/IP_3-dependent and connecting the park mode and the drive mode (1). We formulate q_{24} and q_{42} as

$$q_{24} = a_{24} + V_{24}(1 - m_{24}h_{24}), \tag{S1}$$

$$q_{42} = a_{42} + V_{42}m_{42}h_{42}, \tag{S2}$$

where m_{24}, h_{24}, m_{42} and h_{42} are the Ca^{2+}-/IP_3-modulated "gating variables". a_{24}, a_{42}, V_{24} and V_{42} are either functions of IP_3 concentration (p, in unit of μM) or constants and are given later. We assume those "gating variables" obey the following differential equations,

$$\frac{dG}{dt} = \lambda_G(G_\infty - G), \quad (G = m_{24}, h_{24}, m_{42}, h_{42}), \tag{S3}$$

where G_∞ is the equilibrium and λ_G is the rate at which the equilibrium is approached. Those equilibria are functions of [Ca^{2+}] (c, in unit of μM) , and are modeled by

$$m_{24\infty} = \frac{c^{n_{24}}}{c^{n_{24}} + k_{24}^{n_{24}}}, \tag{S4}$$

$$h_{24\infty} = \frac{k_{-24}^{n_{-24}}}{c^{n_{-24}} + k_{-24}^{n_{-24}}}, \tag{S5}$$

$$m_{42\infty} = \frac{c^{n_{42}}}{c^{n_{42}} + k_{42}^{n_{42}}}, \tag{S6}$$

$$h_{42\infty} = \frac{k_{-42}^{n_{-42}}}{c^{n_{-42}} + k_{-42}^{n_{-42}}}. \tag{S7}$$

Hence, we have

$$q_{24\infty} = a_{24} + V_{24}(1 - m_{24\infty}h_{24\infty}), \tag{S8}$$

$$q_{42\infty} = a_{42} + V_{42}m_{42\infty}h_{42\infty}. \tag{S9}$$

The expressions of as, Vs, ns and ks are chosen as follows so that Eq. S8 and Eq. S9 give good fits to the experimental values of q_{24} and q_{42} shown in Fig. S1,

$$V_{24} = 60 + 437/(p^3 + 1.73), \qquad a_{24} = 1 + 7.5/(p^2 + 0.25),$$

$$V_{42} = 100, \qquad a_{42} = 1.8p^2/(p^2 + 0.34),$$

$$n_{24} = 6.3 + 1.72p^2/(p^2 + 1.44), \qquad k_{24} = 0.48 + 0.1/(p^2 + 1.44),$$

$$n_{-24} = 8.2p^2/(p^2 + 2.25), \qquad k_{-24} = 79.75 + 25/(p^2 + 1.44),$$

$$n_{42} = 5.9 + 7.6/(p^2 + 1.44), \qquad k_{42} = 0.4 + 0.26p^4/(p^4 + 168),$$

$$n_{-42} = 3.2 + 4.88p^2/(p^2 + 1.69), \quad k_{-42} = 0.17 + 70p^3/(p^3 + 274.6).$$

Parameter	Value/Units	Parameter	Value/Units
q_{12}	1240 s^{-1}	q_{21}	88 s^{-1}
q_{23}	3 s^{-1}	q_{32}	69 s^{-1}
q_{26}	10500 s^{-1}	q_{62}	4010 s^{-1}
q_{45}	11 s^{-1}	q_{54}	3330 s^{-1}

TABLE S1: All the transition rates in the Siekmann model except q_{24} and q_{42} (1).

Parameter values of the puff model

Parameter values of the puff model (Eqs. 11–13 in the main text) are given in Table S2.

Estimations of $\lambda_{m_{24}}$, $\lambda_{h_{24}}$, $\lambda_{m_{42}}$ and $\lambda_{h_{42}}$ based on non-stationary single channel data

The rates $\lambda_{m_{24}}$, $\lambda_{h_{24}}$ and $\lambda_{m_{42}}$ in Eq. S3 are evaluated based on the non-stationary single channel data from (4) wherein latency distributions of mode-switch of an IP_3R in response to a sudden step change of $[Ca^{2+}]$ are measured. Considering the data and the IP_3R model together, we can easily see that different changes of $[Ca^{2+}]$ actually reveal different values of the λs. For example, A step increase of $[Ca^{2+}]$ from 10 nM to 2 μM leads to a mode switch of an IP_3R

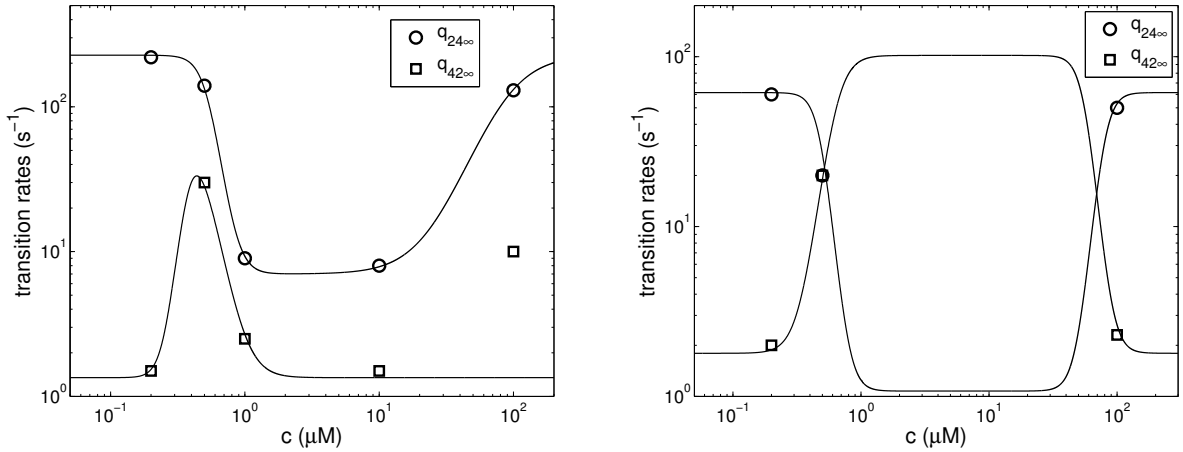

(a) 100 μM ATP and 1 μM IP_3 (b) 100 μM ATP and 10 μM IP_3

FIGURE S1: Stationary transition rates, q_{24} and q_{42}, as functions of $[Ca^{2+}]$. Circles and squares represent the means of q_{24} and q_{42} distributions computed by MCMC simulation (also see (1)). The corresponding fitting curves are produced using Eqs. S4 – S9.

Parameter	Value/Units	Parameter	Value/Units
c_0	0.1 μM	V_d	4000 $\mu\text{M}\cdot\text{s}^{-1}$
J_{increase}	200 $\mu\text{M}\cdot\text{s}^{-1}$	K_d	12 μM
J_{leak}	33 $\mu\text{M}\cdot\text{s}^{-1}$	k_{on}	150 $\mu\text{M}^{-1}\cdot\text{s}^{-1}$
B_{fluo4}	20 μM	k_{off}	300 s^{-1}
c_h	120 μM		

TABLE S2: Parameter values for Eqs. 11–13 in the main text. Parameters relating to fluo-4 are obtained from (2). Resting $[Ca^{2+}]$, c_0, is set to be a typical value of 0.1 μM. c_h is obtained from (3). The remainder of the parameters are determined by requiring physiologically realistic simulations.

from the park mode (or some undetected inactivation mode, as no stationary single channel data at 10 nM $[Ca^{2+}]$ is provided) to the drive mode. During the process, activation latency is solely influenced by the activation of m_{42} (as h_{42} is nearly constant in this range of $[Ca^{2+}]$), which therefore tells us that the value of $\lambda_{m_{42}}$ could be roughly estimated if we can generate a simulated latency distribution in good agreement with the experimental data. Fig. S2a shows the activation latency histogram using $\lambda_{m_{42}} = 100\ \text{s}^{-1}$. It exhibits a good agreement on the range and the location of the peak with the experimental histogram in (4) except showing a smaller dispersion.

Similarly, $\lambda_{m_{24}}$ and $\lambda_{h_{24}}$ are roughly estimated to be 100 s^{-1} and 40 s^{-1} using Fig. S2b and Fig. S2c respectively. We note that experimental latency histogram for $\lambda_{h_{24}}$ clearly contains more than one peak which the current two-mode IP_3R model cannot achieve. To make sure

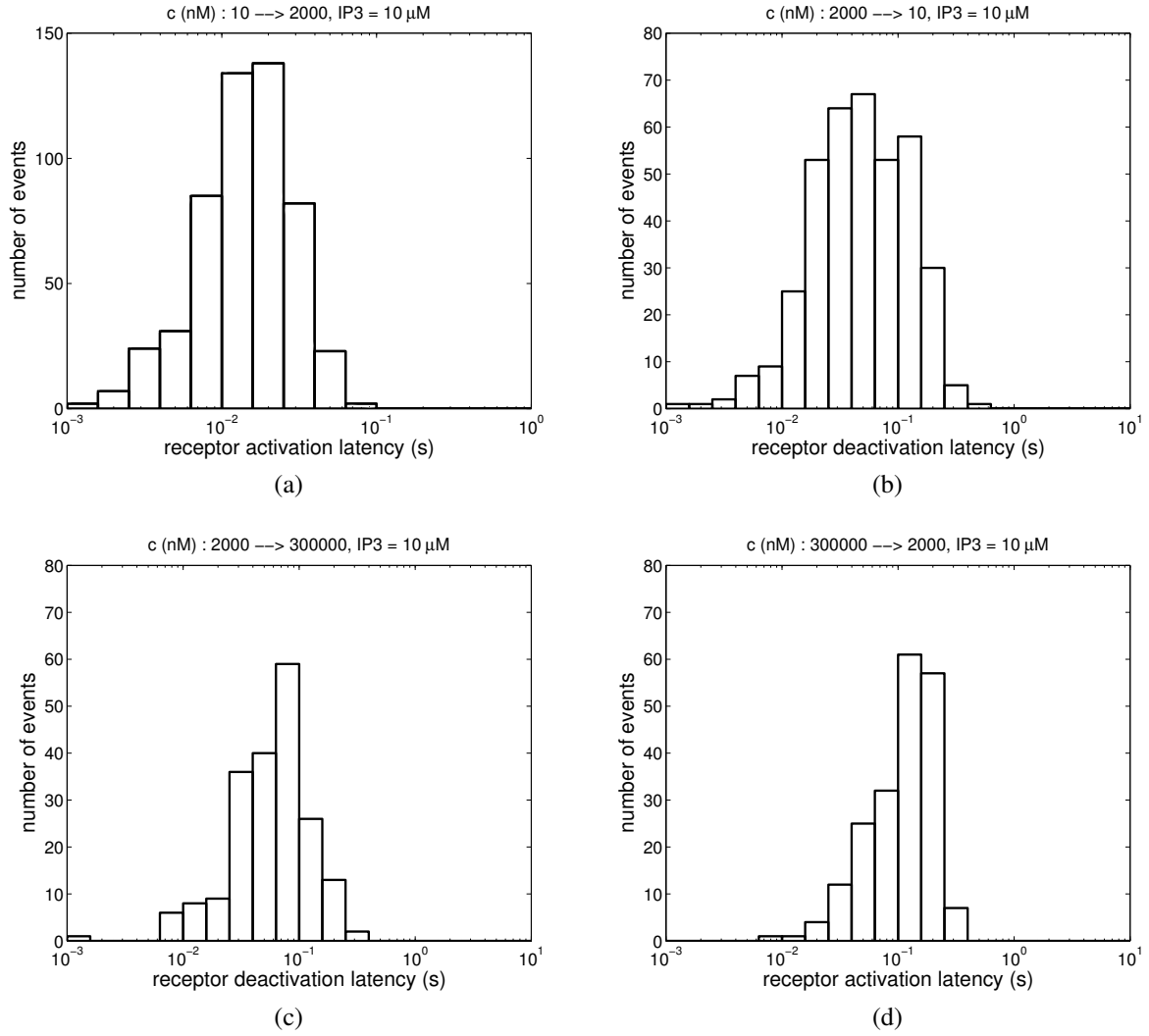

FIGURE S2: Simulated latency histograms for different step changes of $[Ca^{2+}]$ labelled in the titles of the subfigures. We set $p = 10$ μM. As mentioned in the main text, the IP_3R model is built at 100 μM ATP. However in the experiments 500 μM ATP is used (4). Here we assume the difference in [ATP] does not contribute significantly changes to q_{24_∞} and q_{42_∞}, and therefore can be ignored.

the IP_3R model captures the most dominant feature, we only consider the largest peak and use it to estimate $\lambda_{h_{24}}$. Possible reasons for explaining the multimodal distribution could be mode changes caused by randomness of IP_3 binding or unbinding or the existence of some undetected inactivation modes at such a high $[Ca^{2+}]$ of 300 μM (which is beyond the range used to get the stationary single channel data (1)).

The estimation of $\lambda_{h_{42}}$ is unsuccessful, as no value can give an acceptable histogram comparable to the experimental data (see Fig. S2d). The possible reasons have been discussed in the main text. Therefore based on puff data from (5), we propose a model of $\lambda_{h_{42}}$ to be

$$\lambda_{h_{42}} = a_{h_{42}} + \frac{V_{h_{42}} c^7}{c^7 + 20^7}, \tag{S10}$$

We choose $V_{h_{42}} = 100$ s^{-1} to represent a fast Ca^{2+}-inhibition. $a_{h_{42}}$ is considered to be a parameter instead of a constant to investigate its effect on IPI distributions (see Fig. 4 in the main text).

Statistics of calcium blips

In our puff model, by letting $N_{IPR} = 1$, we can simulate blips and their statistics. Similar to IPI, interblip interval (IBI) is the waiting time between successive blips. Fig. S3a shows the IBI distribution is almost an exponential, demonstrating that average recovery time of an IP_3R from self-inhibition is far shorter than average IBI.

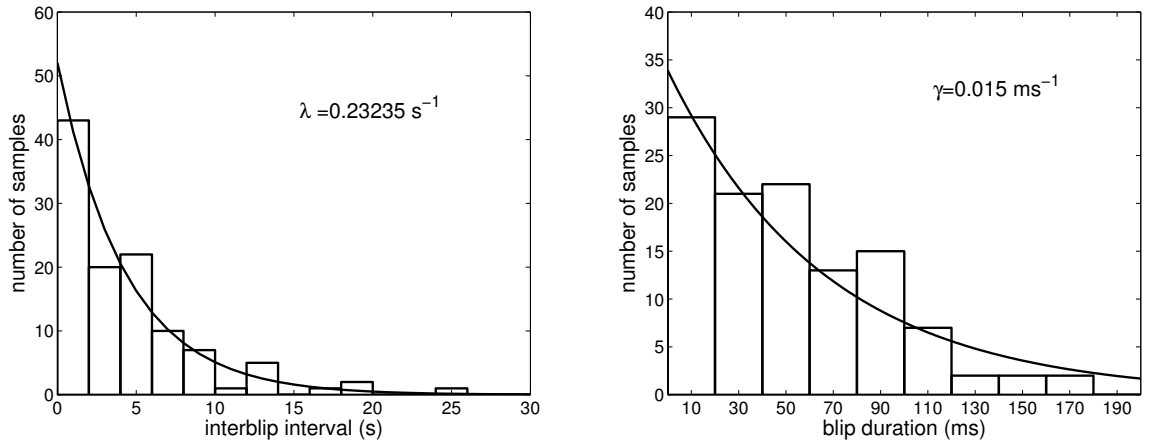

(a) (b)

FIGURE S3: Interblip interval and blip duration distributions obtained by model simulation. We set $p = 0.2$ μM and $a_{h_{42}} = 1$ s^{-1} for both cases. (a) The IBI distribution is fit by Eq. 15 with a λ of about 0.23 s^{-1}. (b) The blip duration distribution is fit by Eq. S11 with a γ of 0.015 ms^{-1}.

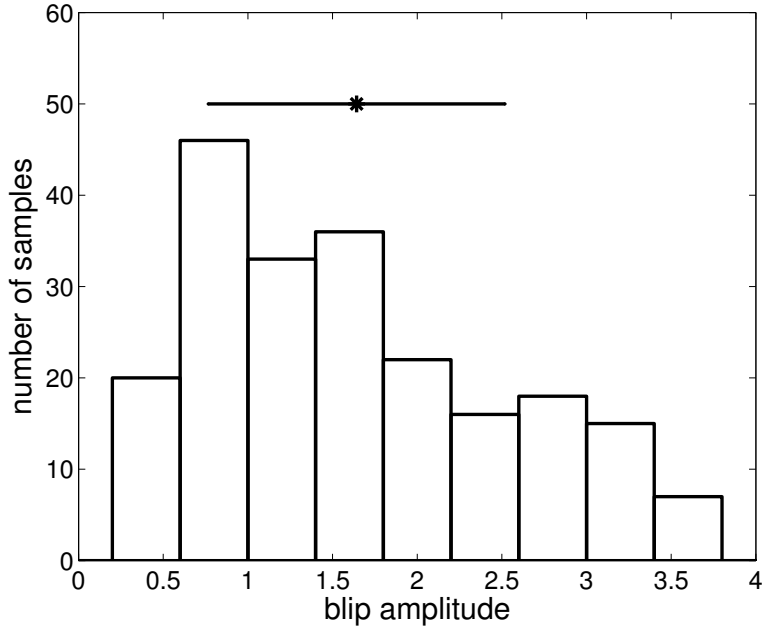

FIGURE S4: Blip amplitude distribution obtained by model simulation. Samples are gathered from two simulations using two IP_3 concentrations, 0.1 μM or 0.2 μM. Blip amplitude is defined to be $(F - F_0)/F_0$ where F and F_0 are defined in the main text. Error bar shows the mean of about 1.6 and standard deviation of about 0.9. We set $a_{h_{42}} = 1$ s^{-1}.

Blip duration distribution is also found experimentally to be an exponential (5), which is qualitatively reproduced by the model (see Fig. S3b). The curve is given by the following exponential distribution,

$$P_{BD} = \gamma e^{-\gamma t}, \tag{S11}$$

which is derived from the below probability density function of puff duration proposed by Thurley *et al.* (6),

$$P_{PD} = N\gamma e^{-\gamma t}(1 - e^{-\gamma t})^{N-1}, \tag{S12}$$

where N is the number of IP_3Rs that are open at the peak of the puff and γ is the average closing rate of a single IP_3R. When $N = 1$, Eq. S12 becomes Eq. S11 containing only one parameter γ.

Fig. S4 shows the blip amplitude distribution with mean of about 1.6 and standard deviation of about 0.9. Based on the mean of blip amplitude, we choose 3 as the sampling threshold to determine which are competent puffs in the puff traces (Fig. 2 in the main text) for statistical analysis.

Interpuff interval distributions for various $a_{h_{42}}$

In the main text, we have shown in Fig. 4 that the fit curves of IPI distributions vary as $a_{h_{42}}$ varies. Each of the fit curves is obtained by choosing appropriate values of λ and/or ξ in Eq. 14 or Eq. 15 so that the corresponding IPI histogram can be fit nicely. Fig. S5 shows some of the fitting results together with the corresponding values of λ and/or ξ.

Dependence of puff amplitude on $a_{h_{42}}$

To understand how $a_{h_{42}}$ influences puff amplitude, we plot average puff amplitude and maximum puff amplitude for different values of $a_{h_{42}}$ in Fig. S6. We find that, as $a_{h_{42}}$ increases, both the average and maximum initially increase but then get saturated at about $a_{h_{42}} = 0.5\ s^{-1}$. Moreover, this trend seems to be independent on IP_3 concentration. The results show that very small recovery rate from Ca^{2+}-inhibition could eventually decrease observed puff amplitude, whereas not too small recovery rate would not significantly change puff amplitude. Therefore, If $a_{h_{42}}$ can be known experimentally, we could then know whether the number of IP_3Rs is severely underestimated by observed puff amplitude and to what extent it is underestimated. Accordingly, if the number of IP_3Rs is known, we could also roughly estimate the range of $a_{h_{42}}$.

Dependence of puff amplitude on IPI

In the main text, model results have shown the preceding puff has definitely an inhibitory effect on the occurrence of the next puff (see Figs. 5 and 7) and this effect comes from the slow recovery of h_{42} (see Fig. 3). This means a long IPI is easier to lead to a larger puff, as most IP_3Rs have been restored to resting states. A more straightforward relation of puff amplitude and IPI can be seen in Fig. S7 wherein puff amplitude is directly plotted in terms of the preceding IPI. We can see in the scatter plot that as the preceding IPI increases, puff amplitude also follows a gradually increasing trend but seems to get saturated when IPI is longer than 2 s. The saturation can be seen clearly in Fig. S8a wherein we group those points

in Fig. S7 in bins of IPI and then calculate average puff amplitude in each bin. This result is qualitatively consistent with the experimental data in (7).

We also find that where the saturation occurs depends on $a_{h_{42}}$. In Fig. S8, we test two cases of $a_{h_{42}}$, 1 s^{-1} (a) and 0.1 s^{-1} (b). Noting that the saturation occurs at about $1 \sim 2$ s for $a_{h_{42}} = 1$ s^{-1} but at about $8 \sim 12$ s for $a_{h_{42}} = 0.1$ s^{-1}, we predict that the saturation should occur at about $1/a_{h_{42}}$. Importantly, this provides a way of estimating the slow recovery rate $a_{h_{42}}$ experimentally, as Fig. S8 can be easily obtained using experimental data.

In addition, we find the following IPI seems to be independent on the preceding puff amplitude by looking at the scatter plot similar to Fig. S7 (results not shown). This could be explained by Fig. 3 in the main text, where we can see the inactivation variable h_{42} will quickly drop down to be very close to 0 during a puff regardless of the puff amplitude. Therefore, the inhibitory effect from preceding puffs with various amplitudes on the following IPIs is nearly identical.

Dependence of puff [Ca^{2+}] amplitude on the number of IP_3Rs at a puff site

As seen in Fig. 8 in the main text, puff amplitude is a piecewise nonlinear function of the number of IP_3Rs (N_{IPR}). However, if using [Ca^{2+}] instead of normalized Ca^{2+}-bound buffer as puff amplitude, we find that average puff [Ca^{2+}] amplitude is linearly related to N_{IPR} (see Fig. S9). This result shows the nonlinear relation of puff amplitude and N_{IPR} in Fig. 8 is caused by the nonlinear relationship between [Ca^{2+}] and Ca^{2+}-bound fluo-4.

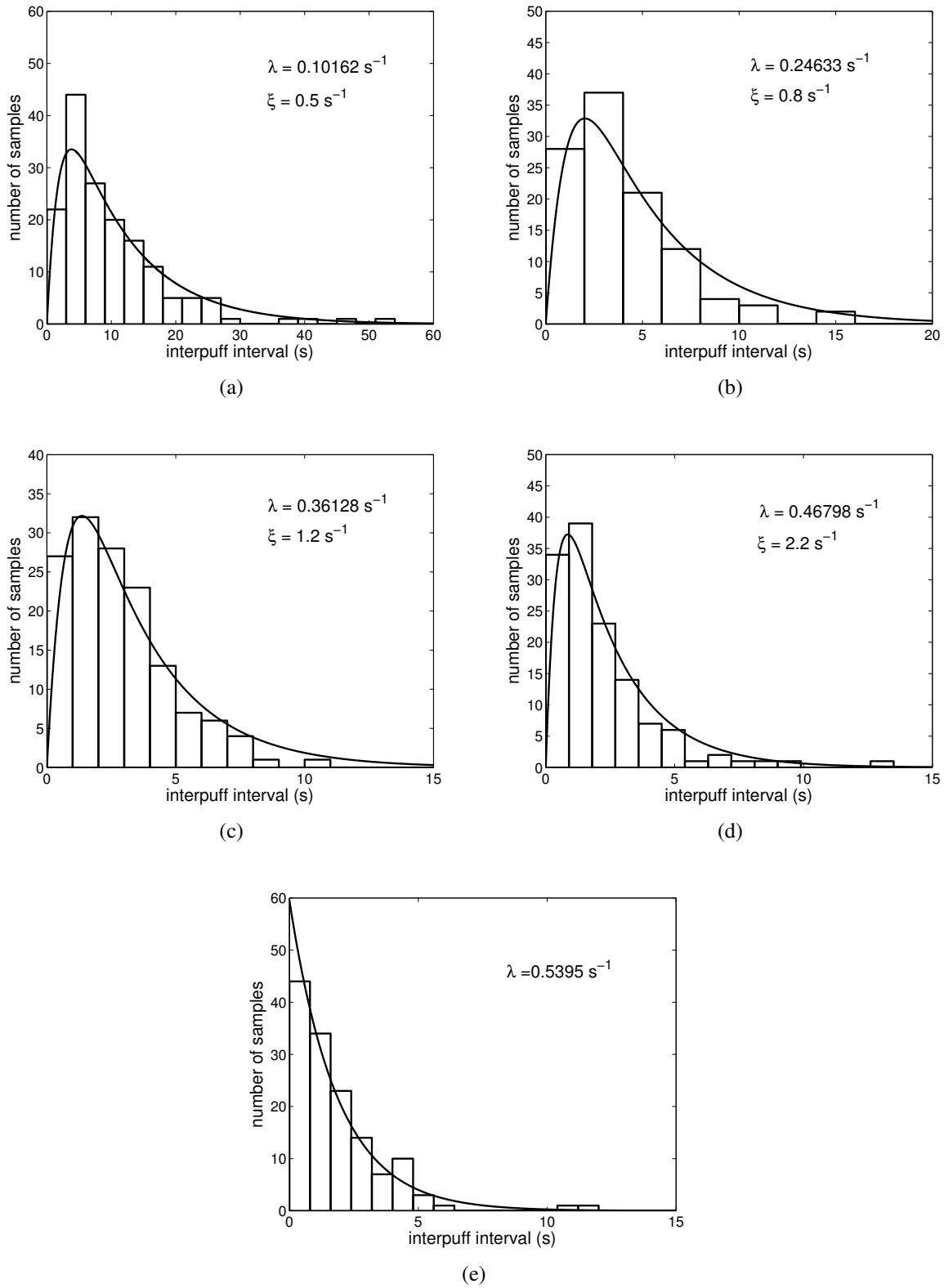

FIGURE S5: Various IPI distributions are well fit by Eq. 14 or Eq. 15 in the main text with appropriate values of λ and/or ξ shown in each of the sub figures. 5 values of $a_{h_{42}}$, 0.1 s^{-1} (a), 0.5 s^{-1} (b), 1 s^{-1} (c), 2 s^{-1} (d) and 5 s^{-1} (e), are chosen. We set $N_{IPR} = 10$ and $p = 0.1$ μM.

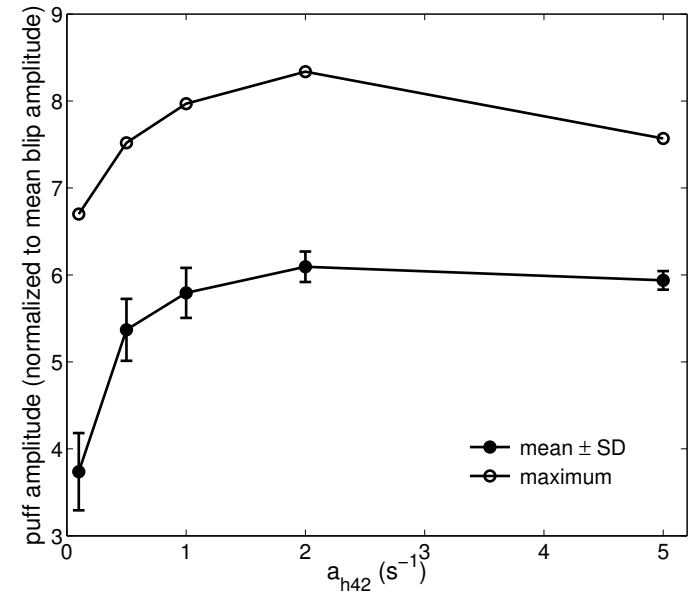

(a)

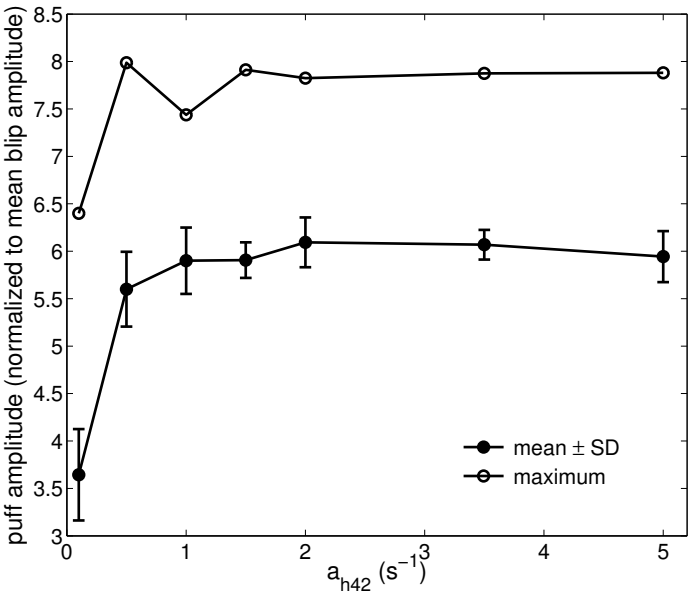

(b)

FIGURE S6: Dependence of puff amplitude on $a_{h_{42}}$. Average puff amplitude (filled circle with error bar) and maximum puff amplitude (empty circle) are plotted for various values of $a_{h_{42}}$. Puff amplitudes have been normalized to the mean blip amplitude of 1.6. We perform two simulations with two different IP_3 concentrations, 0.05 μM (a) and 0.1 μM (b), respectively. We set $N_{IPR} = 10$.

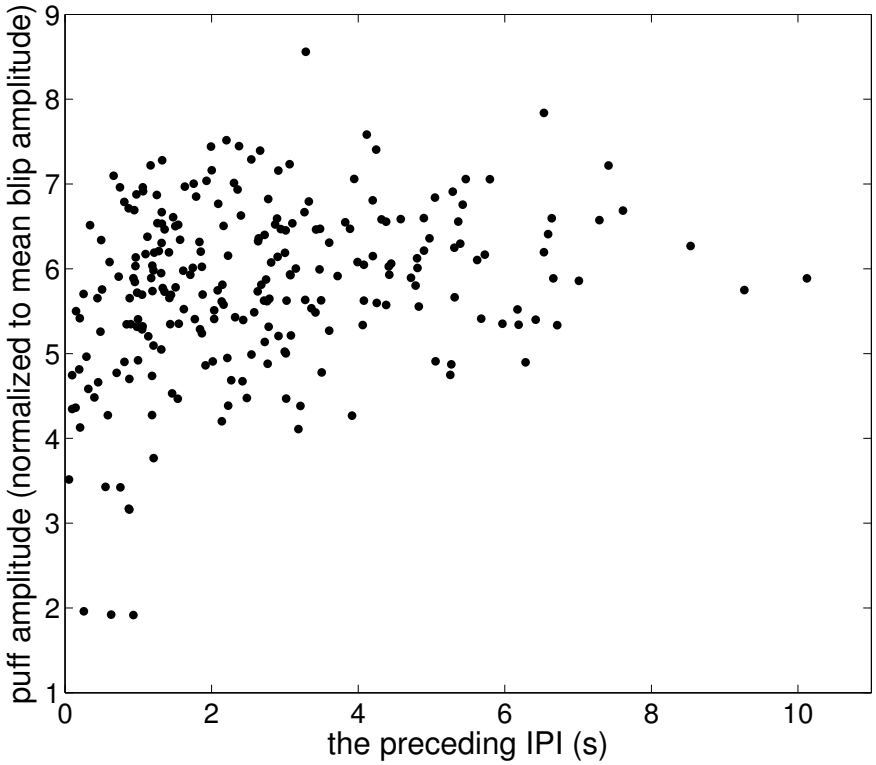

FIGURE S7: Scatter plot shows the relation of puff amplitude and the preceding IPIs. Puff amplitude has been normalized to the mean blip amplitude of 1.6. We set $N_{IPR} = 10$, $p = 0.1$ μM and $a_{h_{42}} = 1$ s^{-1}.

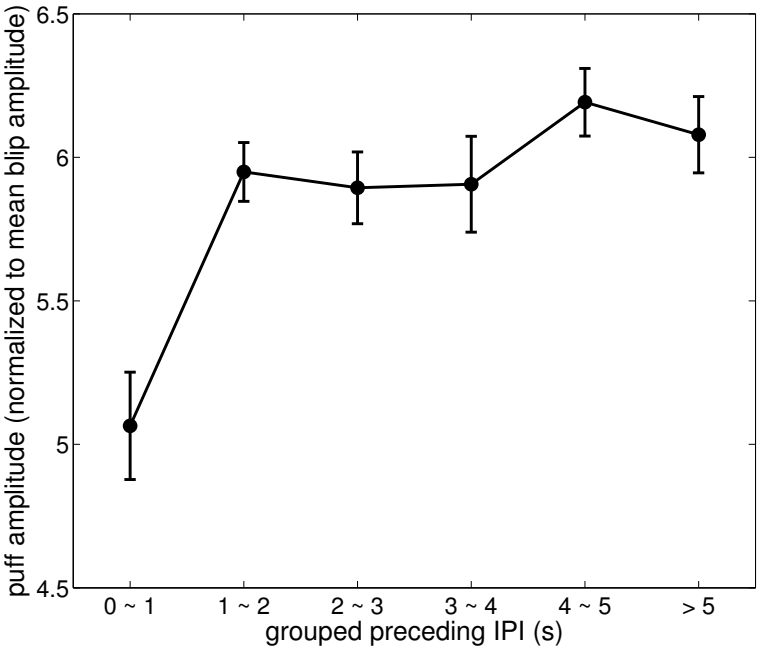

(a)

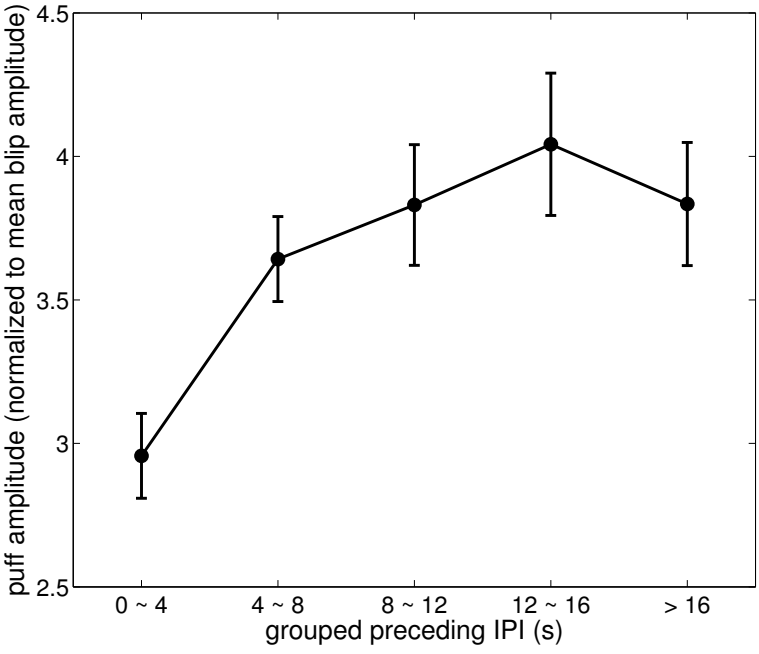

(b)

FIGURE S8: Average puff amplitude is plotted in terms of grouped preceding IPIs. Simulations are performed for two different values of $a_{h_{42}}$, 1 s^{-1} (a) and 0.1 s^{-1} (b). Puff amplitude has been normalized to the mean blip amplitude of 1.6. In each bin, there are about $10 \sim 30$ samples. Results are expressed to be mean $\pm$ SE. We set $N_{IPR} = 10$ and $p = 0.1$ μM.

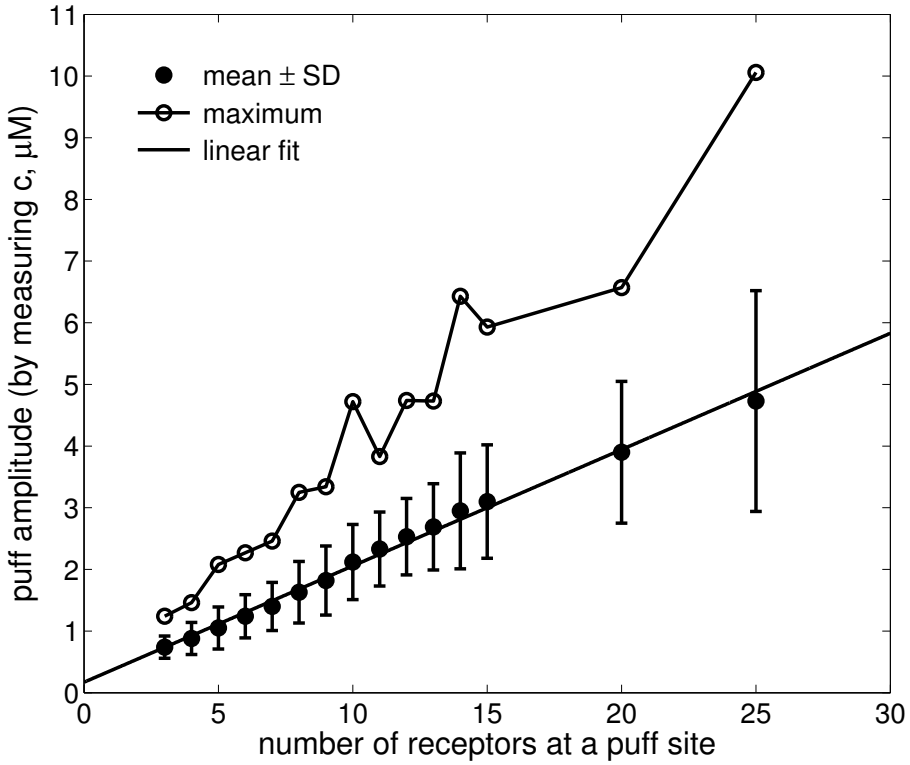

FIGURE S9: Dependence of average puff amplitude (filled circle) and the largest puff amplitude (empty circle) expressed by $[Ca^{2+}]$ on the number of IP_3Rs at a puff site. A linear fit to the average puff $[Ca^{2+}]$ amplitude is shown by the solid line. We set $p = 0.1$ μM and $a_{h_{42}} = 1$ s^{-1}.

References

1. Siekmann, I., L. E. Wagner, D. I. Yule, E. J. Crampin, and J. Sneyd. 2012 A kinetic model for IP_3R type I and type II accounting for mode changes. *Biophys. J.* 103: 658–668.

2. Shuai, J., H. J. Rose, and I. Parker. 2006. The number and spatial distribution of IP_3 receptors underlying calcium puffs in *Xenopus* oocytes. *Biophys. J.* 91: 4033–4044.

3. Rüdiger, S., J. Shuai, and I. Solovey. 2010. Law of mass action, detailed balance, and the modeling of calcium puffs. *Phys. Rev. Lett.* 105: 048103.

4. Mak, D.O.D., J. E. Pearson, K. H. Cheung, S. Datta, M. Fernandez-Mongil, and K. J. Foskett. 2007. Rapid ligand-regulated gating kinetics of single IP_3R Ca^{2+} release channels. *EMBO Reports* 8: 1044–1051.

5. Smith, I. F., and I. Parker. 2009. Imaging the quantal substructure of single IP_3R channel activity during Ca^{2+} puffs in intact mammalian cells. *Proc. Natl. Acad. Sci. USA.* 106(15): 6404–6409.

6. Thurley, K., A. Skupin, R. Thul, and M. Falcke. 2012. Fundamental properties of Ca^{2+} signals. *Biochimica et Biophysica Acta.* 1820(8): 1185–1194.

7. Fraiman, D., B, Pando, S. Dargan, I. Parker, and S. P. Dawson. 2006. Analysis of puff dynamics in oocytes: interdependence of puff amplitude and interpuff interval. *Biophys. J.* 90: 3897–3907.